Using Neural Networks for Fast Reachable Set Computations

Frank Jiang*, Glen Chou*, Mo Chen*, Claire J. Tomlin *

arXiv:1611.03158v1 [cs.LG] 10 Nov 2016

ABSTRACT

Hamilton-Jacobi (HJ) reachability is a powerful tool that provides performance and safety guarantees for dynamical systems. Unfortunately, using the state-of-the-art dynamic programming-based approaches, HJ reachability is intractable for systems with more than five dimensions because its computational complexity scales exponentially with system dimension. To sidestep the curse of dimensionality, we propose an algorithm that leverages a neural network to approximate the minimum time-to-reach function to synthesize controls. We show that our neural network generates near optimal controls which are guaranteed to successfully drive the system to a target state. Our framework is not dependent on state space discretization, leading to a significant reduction in computation time and space complexity in comparison with dynamic programming-based approaches. Using this grid-free approach also enables us to plan over longer time horizons with relatively little additional computation overhead. Unlike many previous neural network reachability formulations, our approximation is conservative and hence any trajectories we generate will be strictly feasible. For demonstration, we specialize our new general framework to the Dubins car model and discuss how the general framework can be applied to other models with higher-dimensional state spaces.

1. INTRODUCTION

In recent years, rapid progress in robotics and artificial intelligence have accelerated the need for efficient path-planning algorithms in high-dimensional spaces. In particular, there has been vast interest in the development of autonomous cars and unmanned aerial vehicles (UAVs) for civilian purposes [3,4,7,21,23,25]. As such systems grow in complexity, development of algorithms that can tractably control them in high-dimensional state spaces will become necessary.

Hamilton-Jacobi (HJ) reachability is a theoretically important and practically powerful tool for analyzing a large range of systems. It has been extensively studied in [5, 9, 20, 22, 27, 30, 35, 36], and successfully applied to many low-dimensional real world systems [12, 16, 30]. The core idea of reachability analysis is to compute the reachable set, which represents the set of states from which the system can be driven into a target set. From the reachable set, the optimal control for reaching the target set can be synthesized. Unfortunately, current state-of-the-art numerical methods for computing reachable sets discretize the state space, resulting in space and time complexities that scale exponentially with the system dimension.

In an effort to overcome the curse of dimensionality, many methods which heavily restrict the system at hand have been proposed. For example, one method requires the system dynamics to be polynomial [18, 26], while another method requires the Hamiltonian to be a function of only the controlled variable [15]. There are also less restrictive methods using projections, approximate dynamic programming, and approximate systems decoupling [11, 28, 31], each with its own limitations in flexibility, scalability, and degree of conservatism.

One of the main drawbacks of reachability analysis and other dynamic programming-based approaches is the need to compute a value function over a large portion of the state space. This is computationally wasteful since the value function, from which the optimal controller is derived, is only needed along a trajectory from the system's initial state to the target set. A more efficient approach would be to only compute the value function local to the trajectory from the initial state to the target set. However, there is no way of knowing where such a trajectory will lie before thoroughly computing the value function.

Methods that exploit machine learning have great potential because they are state discretization-free and do not depend on the dynamic programming principle. Unfortunately, many machine learning techniques cannot make the guarantees provided by reachability analysis. For instance, [8] and [24] use neural networks (NNs) as nonlinear optimizers to synthesize trajectories which may not be dynamically feasible. The authors in [2] propose a supervised learning-based algorithm that depends heavily on feature tuning and design, making its application to high-dimensional problems cumbersome. In [17] and [32], the authors successfully use NNs for approximating the value function, but the approximation is not guaranteed to be conservative.

In this paper, we attempt to combine the best features of both reachability and machine learning using an NN-based algorithm. Our proposed grid-free method conservatively

** All three authors contributed equally to this work.

ACM ISBN 978-1-4503-2138-9.
DOI: 10.1145/1235

approximates the time-to-reach (TTR) representation of a reachable set in only a region around a feasible trajectory. Unlike previous machine learning techniques, our technique guarantees a direction of conservatism, and unlike previous dynamic programming-based methods, our approach involves an NN that effectively figures out the relevant region in which a value function is required. Our contributions will be presented as follows:

- In Section 2, we summarize HJ reachability as well as the formalisms used for this work.
- In Sections 3 and 4, we present the two phases of our proposed algorithm and the underlying design choices. In particular, we show the guaranteed feasibility and conservatism properties of our framework.
- In Section 5, we develop, apply, and validate our method on the Dubins car model and discuss our numerical results. Here, we will illustrate our guaranteed-conservative approximation of the TTR function, and the resulting near-optimal trajectories.
- Finally, in Section 6, we discuss future directions, including applying the method to higher-dimensional systems.

2. PROBLEM FORMULATION

In this section, we will first provide an overview of HJ reachability theory as well as some definitions essential to express our main results. Afterwards, we will briefly discuss the goals of this paper.

2.1 Background

2.1.1 System Dynamics

Consider a dynamical system governed by the following ordinary differential equation (ODE):

$$\dot{x} = f(x, u), \quad u \in \mathcal{U} \tag{1}$$

Here, $x \in \mathbb{R}^n$ is the state of the system and the control function $u(\cdot)$ is assumed to be drawn from the set of measurable functions[1]. Let us further assume that the system dynamics $f : \mathbb{R}^n \times \mathcal{U} \to \mathbb{R}^n$ are uniformly continuous, bounded, and Lipschitz continuous in x for fixed u. Denote the function space from which f is drawn as $\mathbb{F}$.

With these assumptions, given some initial state x, initial time t_0, and control function $u(\cdot) \in \mathbb{U}$, there exists a unique trajectory solving (1). We refer to trajectories of (1) starting from state x and time t_0 as $\xi(t; x, t_0, u(\cdot))$. Trajectories satisfy an initial condition and (1) almost everywhere:

$$\begin{aligned} \frac{d}{dt}\xi^f(t; x, t_0, u(\cdot)) &= f(\xi^f(t; x, t_0, u(\cdot)), u(t)) \\ \xi^f(t_0; x, t_0, u(\cdot)) &= x \end{aligned} \tag{2}$$

Throughout the paper, we will extensively use the backward-time dynamics $\dot{x} = -f(x, u)$, whose trajectories will be denoted $\xi^{-f}(t; x, t_0, u(\cdot))$. Note that

$$x_f = \xi^f(t_f; x_0, t_0, u(\cdot)) \Leftrightarrow x_0 = \xi^{-f}(t_f; x_f, t_0, u(\cdot)) \tag{3}$$

2.1.2 Minimum Time-To-Reach

In this paper we consider a particular formulation of the reachability problem, which we will refer to as the time-to-reach (TTR) problem. In this context, we would like to find the minimum time the system needs to reach a target set $\mathcal{L}$ from a starting point x. Without loss of generality (WLOG), we assume the starting time is $t_0 = 0$, and define the TTR function as follows:

DEFINITION 1. ***Time-to-reach function.***

$$\phi(x) = \min_{u(\cdot)\in\mathbb{U}} \min_{t} \{\xi^f(t; x, 0, u(\cdot)) \in \mathcal{L}\} \tag{4}$$

There are many HJ formulations for obtaining the TTR function $\phi(x)$ [6, 10, 30]. For example, $\phi(x)$ is the viscosity solution [13] of the following HJ PDE [37]:

$$\begin{aligned} \min_{u\in\mathcal{U}}\{-\nabla\phi(x) \cdot f(x, u) - 1\} = 0 \ \forall x \notin \mathcal{L} \\ \phi(x) = 0 \ \forall \phi \in \mathcal{L} \end{aligned} \tag{5}$$

After obtaining the solution $\phi(x)$, the optimal control, which drives the system to the set $\mathcal{L}$ in minimum, can be extracted as follows:

$$u^*(x) = \arg\min_{u\in\mathcal{U}} \nabla\phi(x) \cdot f(x, u) \tag{6}$$

In general, numerical methods for finding $\phi(x)$ such as the one outlined in [37], as well as many others [29, 33, 34], involve representing the state space on a grid, leading to an exponentially scaling computation complexity with respect to the system dimension.

2.2 Goal

In this paper, we seek to overcome the exponentially scaling computation complexity. Our approach is inspired by two inherent challenges that dynamic programming-based methods face.

First, since only relatively mild assumptions are placed on the system dynamics (1), optimal trajectories are *a priori* unknown and could essentially trace out any arbitrary path in the state space. Dynamic programming ignores this issue by considering *all possible* behaviors of the trajectory. Numerical methods are needed to obtain dynamic programming solutions, leading to the necessity of discretizing the state space.

Second, in a practical setting, the system starts at some particular state x. Thus, the optimal control, and in particular $\nabla\phi(x)$ in (6), is needed *only along* the optimal trajectory. However, again, since the optimal trajectory is *a priori* unknown, dynamic programming-based approaches resort to computing $\phi(x)$ over a very large portion of the state space so that the $\nabla\phi(x)$ is available regardless of where the optimal trajectory happens to be.

In this paper, we propose a method that, in contrast to dynamic programming-based methods,

1. has a sub-exponential complexity scaling with repsect to the state space dimension;

[1] A function $f : X \to Y$ between two measurable spaces (X, Σ_X) and (Y, Σ_Y) is said to be measurable if the preimage of a measurable set in Y is a measurable set in X, that is: $\forall V \in \Sigma_Y, f^1(V) \in \Sigma_X$, with $\Sigma_X, \Sigma_Y \sigma$-algebras on X, Y.

2. is applicable to higher-order or more complex systems without changing the NN architecture or dynamic training procedure;

3. generates an approximate TTR function from which a controller that drives the system to the target can be synthesized;

4. guarantees a direction of conservatism, despite the use of an NN.

We enforce 1) by avoiding operations that exhaustively search the state space. As seen in Sections 3.2 and 3.3, the training and final data sets are either generated randomly or outputted by the NN, both constant time operations. Furthermore, we rely on NNs being universal function approximators [14] to make our method general to the system dynamics, thus satisfying 2). While our method does have some limitations, as discussed at the end of Section 3.1, we do not believe that these limitations are restrictive in the context of reachability analysis. Our post processing of the NN outputs outlined in Section 4 satisfies 3). Finally, we use the dynamics of the system to ensure our final output satisfies 4); this is detailed in Section 3.3.

Our method overcomes the challenges faced by dynamic programming-based in two phases: the NN training phase, which allows the NN to learn the inverse backward system dynamics, and the controller synthesis phase, which uses the NN to obtain TTR approximations that can be used to synthesize a controller.

3. NEURAL NETWORK TRAINING PHASE

Given a target state $x_{\mathcal{L}}$ and assuming the system starts at some initial state $\bar{x}$, we want to design an NN that can produce a control function $u(\cdot)$ that drives the system from $\bar{x}$ to $x_{\mathcal{L}}$. Equivalently, $u(\cdot)$ should drive the backward system from $x_{\mathcal{L}}$ to $\bar{x}$. Since the NN is not perfect, it can only be expected to produce approximate control functions $\hat{u}_i(\cdot)$ that drive the backward system from $x_{\mathcal{L}}$ to $\hat{x}_i$. If the NN is well-trained, then each $\hat{x}_i$ would be very close to $\bar{x}$.

More concretely, consider the inverse backward dynamics of the system, denoted $g : \mathbb{R}^n \times \mathbb{F} \to \mathbb{U}$, and defined to be

$$g(\bar{x}, x_{\mathcal{L}}; -f(\cdot,\cdot)) = u^*(\cdot) \tag{7}$$

where the optimal control $u^*(\cdot)$ is defined in the time interval $[0, \phi(\bar{x})]$. Given the $u^*(\cdot)$, we have $\bar{x} = \xi^{-f}(\phi(\bar{x}); x_{\mathcal{L}}, 0, u^*(\cdot))$.

Our NN is an approximation to g, and we will denote the NN as $\hat{g}$. Let $\hat{u}(\cdot)$ be the control produced by $\hat{g}$, and let the time interval for which $\hat{u}(\cdot)$ is defined be denoted $[0, \hat{T}]$. In general, applying $\hat{u}(\cdot)$ brings the backward system from $x_{\mathcal{L}}$ to some $\hat{x} \neq \bar{x}$. Regardless of what $\hat{x}$ happens to be, $\hat{T}$ is guaranteed to be an over-approximation of $\phi(\hat{x})$: $\hat{\phi}(\hat{x}) = \hat{T} \geq \phi(\hat{x})$. This is because the point $\hat{x}$ is generated from simulation, and therefore the corresponding TTR $\hat{T}$ cannot possibly be smaller than the optimal TTR $\phi(\hat{x})$. If we can obtain the $\hat{\phi}(x)$ for many values of x near $\bar{x}$, then we would be able to synthesize a suboptimal control via (6).

Denote the maximum value of ϕ we would like to approximate as $\bar{T}$. To reduce the space in which the NN needs to look for candidate control functions, we assume that $\hat{u}(\cdot)$ returned by the NN is composed of two finite sequences $\{u^j\}_{j=1}^K, \{\tau^j\}_{j=1}^K$ called the sequence of control primitives and the sequence of time durations respectively. Mathematically, the control function $\hat{u}(\cdot)$ is of the form

$$\hat{u}(t) = \begin{cases} u^1, & t \in [0, \tau^1] \\ u^2, & t \in [\tau^1, \tau^1 + \tau^2] \\ \dots & \\ u^K, & t \in [\sum_{j=1}^{N-1} \tau^j, \sum_{j=1}^{N} \tau^j] \end{cases} \tag{8}$$

Note that $\sum_{j=1}^K \tau^j = \hat{T} \leq \bar{T}$. Since we will only use the control to obtain the approximation $\hat{\phi}(\cdot)$ and not for actually controlling the system, we do not need the generated controls to be extremely accurate or continuous, as we will explain in Sections 3.3 and 4.

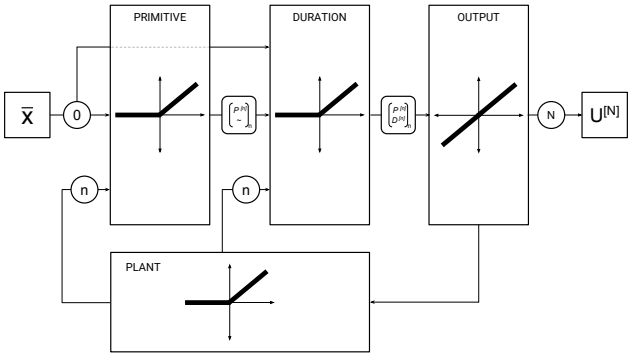

Figure 1: Four-layer RRNN which takes input states and outputs discretized control.

3.1 Neural Network Architecture

We propose a rectified linear unit recurrent NN (RRNN) with the following structure:

$$\begin{aligned} \text{Primitive Layer: } & P^{[n]} = \psi(W_P \cdot X^{[n]} + b_P) \\ \text{Duration Layer: } & D^{[n]} = \psi(W_{D_1} \cdot P^{[n]} + W_{D_2} \cdot X^{[n]} + b_D) \\ \text{Control Layer: } & U^{[n]} = W_L \cdot D^{[n]} + b_L \\ \text{Plant Layer: } & X^{[n+1]} = \psi(W_X \cdot U^{[n]} + b_X) \end{aligned}$$

where ψ is the positive rectifying function defined as $\psi(a) = \max(0, a)$ and $n = 0, 1, \dots, N$. The input of the RRNN is $\bar{x}$ ($X^{[0]} = \bar{x}$), and the output is some $\hat{u}(\cdot)$ ($U^{[N]} = \hat{u}(\cdot)$), that approximately brings the system from $\bar{x}$ to $x_{\mathcal{L}}$. The parameters we learn through training are the weights W_P, W_{D_1}, W_{D_2}, W_L, W_X and biases b_P, b_D, b_L, b_X. All weights and biases will be collectively denoted $\mathbb{W}$. The training is performed with the mean squared error as the cost function.

As already mentioned, the primitive layer takes a state as input and computes a control primitive. The duration layer takes in the primitive layer's output and the same input state, and outputs a time duration. This time duration is then passed through the control (also called output) linear layer, which outputs the sequences $\{u^j\}, \{\tau^j\}$ representing the control function $\hat{u}(\cdot)$. Afterwards, the control function is fed into the plant layer, which attempst to encode the backward dynamics $-f$. The plant's output state, $X^{[n+1]}$, is then fed back to the primitive layer.

In order to ensure W_X, or the plant layer weights, are accurate, they are initialized by an isolated supervised train-

ing process. The training set we use to perform the isolated training is detailed in 3.2. Intuitively, by initializing W_X, we are giving the RRNN an initial idea of the backward dynamics before learning the inverse backward dynamics. Explicitly, the RRNN can be written as

$$\hat{g}(\bar{x}, x_{\mathcal{L}}; -f(\cdot,\cdot), \mathbb{W}) = \hat{u}(\cdot) = U^{[N]} \tag{9}$$

where $\hat{u}(\cdot)$ is given in the form of the sequences $\{u^j\}, \{\tau^j\}$, from which we can obtain $\hat{T} = \sum_{j=1}^{N} \tau^j$.

In the next section, we discuss a method for generating training data for the RRNN.

3.2 Initial Training Data Generation

We first train the RRNN without knowledge of $\bar{x}$ to initialize the dynamic training algorithm described in the next section. To do this, we require training examples in the form of $\{(\hat{x}_i, \hat{u}_i(\cdot))\}$ that sufficiently capture the behavior of the system dynamics. $\{\hat{x}_i\}$ is randomly generated using an accept-reject algorithm similar to the one in [17] and described in Alg. 1, which outputs a boolean variable A indicating whether to accept some state x. A state x, an accept region $\mathcal{R}$, and a decay rate λ are required as inputs.

In Alg. 1, we first compute x_{proj}, the Euclidean projection of the state x onto the set $\mathcal{R}$ as follows:

$$x_{\text{proj}} = \min_{x'} \|x' - x\|_2 : x' \in \mathcal{R} \tag{10}$$

Using the accept-reject algorithm, we generate two training sets. The larger data set $\mathcal{D}_1$ is used for supervised training of the plant layer (the weights W_X), and is generated with a large accept region until a certain number of points are accepted. The smaller dataset $\mathcal{D}_2$ is used to initialize the dynamic training algorithm, and is generated with a smaller accept region.

Algorithm 1 Exponential Filter

1: **Result**: A
2: **Inputs**: x, $\mathcal{R}$, λ
3: compute x_{proj} via (10)
4: generate β uniformly from $[0, \lambda]$
5: **if** $x \in \mathcal{R}$ **then**
6: $\quad A = \text{true}$
7: **else**
8: $\quad$ **if** $\beta \leq \lambda e^{-\lambda \|x - x_{\text{proj}}\|_2}$ **then**
9: $\quad\quad A = \text{true}$
10: $\quad$ **else**
11: $\quad\quad A = \text{false}$
12: $\quad$ **end if**
13: **end if**

3.3 Dynamic Training

The dynamic training procedure is designed to selectively prune the RRNN's inputs in order to bias its resulting controls $\hat{u}(\cdot)$ towards bringing the backward system from $x_{\mathcal{L}}$ to $\bar{x}$. The result of dynamic training is a set of states $\mathcal{X}$ which contains many points near $\bar{x}$, and the corresponding set of controls $\mathcal{V}$ that drives the system from the states $\mathcal{X}$ to $x_{\mathcal{L}}$. The procedure is shown in detail in Alg. 2, and can bebroken down into the following steps:

1. Initialization (lines 3-5)

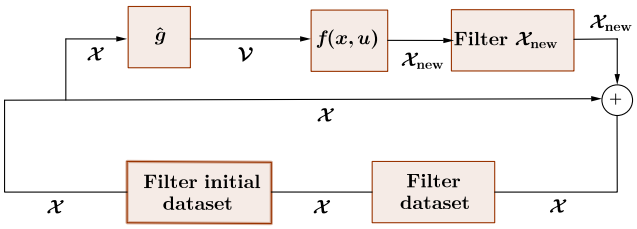

Figure 2: Block diagram representation of main dynamic training loop (lines 8-47).

2. Train RRNN by updating the weights $\mathbb{W}$ (line 8)
3. Filter RRNN outputs $\mathcal{X}_{\text{new}}$ in current iteration (lines 9-24)
4. Filter RRNN training set $\mathcal{X}$ from previous iterations (line 25-32)
5. Filter data from initial training set $\mathcal{X} \cap \mathcal{D}_2$, and then update the training sets $\mathcal{X}, \mathcal{V}$. (line 33-47)
6. Repeat steps 2-5 until either a maximum iteration limit is reached or enough states in $\mathcal{X}$ are within a distance of ϵ to $\bar{x}$.

3.3.1 *Initialization*

Before the initialization of Alg. 2, the RRNN's plant layer has been trained on $\mathcal{D}_1$ in isolation.

Dynamic training initialization requires the following inputs: the dataset $\mathcal{D}_2$, the state $\bar{x}$, the desired accept region radius ϵ, the number of desired samples M_ϵ in that region, the iteration iter_{ps} after which we want to activate pruning of the $\mathcal{D}_2$, the maximum desired number of states $M_{\max}$ near $\bar{x}$, and the maximum number of training iterations $\text{iter}_{\max}$. In addition, three different accept regions, denoted $\mathcal{R}_{\text{O}}, \mathcal{R}_{\text{PS}}, \mathcal{R}_{\text{ITS}}$, are required. Suggestions on choosing $\mathcal{R}_{\text{O}}, \mathcal{R}_{\text{PS}}, \mathcal{R}_{\text{ITS}}$ for the Dubins car example are given in Section 5.4.1.

We first initialize $\mathcal{X}$ to be $\mathcal{X} = \mathcal{D}_2$. Next, we uniformly sample M_ϵ states within a distance of ϵ to $\bar{x}$ to produce a set of states denoted $\mathcal{E}$.

3.3.2 *Neural Network and Output Filtering*

We now input the states in $\mathcal{E}$ to the RRNN to produce M_ϵ controls, $\{\hat{u}_i(\cdot)\}_{i=1}^{M_\epsilon}$, from which we compute the resulting set of states $\{\hat{x}_i\}_{i=1}^{M_\epsilon}$ according to the dynamics (1). Next, we add $\{\hat{x}_i\}_{i=1}^{M_\epsilon}$ to a temporary set denoted $\mathcal{X}_{\text{new}}$.

To avoid training on data points far from the target, the exponential accept-reject filter (Alg. 1) is applied to the states in $\mathcal{X}_{\text{new}}$, with the accept region $\mathcal{R}_{\text{O}}$.

$\mathcal{R}_{\text{O}}$ depends on the system dynamics and is generally tuned; usually, it should contains states that could lie on a feasible path from $\bar{x}$ to $x_{\mathcal{L}}$. For general high-dimensional systems with complicated dynamics, it may be difficult to estimate $\mathcal{R}_{\text{O}}$, and $\mathcal{R}_{\text{O}}$ can be tuned based on the performance of RRNN.

3.3.3 *Previous State Filtering*

This part of the algorithm filters out states from previous training iterations using the accept region $\mathcal{R}_{\text{PS}}$. Such a filter reduces the likelihood that old data from many iterations ago affect the performance of the RRNN adversely.

3.3.4 Initial Training Set Filtering

In early iterations of training, states from the initial training set $\mathcal{D}_2$ provide the general information about the system dynamics needed for the RRNN to explore the state space. However, after sufficient exploration, the RRNN gains information about the system dynamics specific for reaching $\bar{x}$; thus, the data in $\mathcal{D}_2$ becomes less important. Hence, once the number of training iterations exceeds a threshold iter_{ps}, we prune states from the $\mathcal{D}_2$ using the accept region denoted by $\mathcal{R}_{\text{ITS}}$, chosen to remove states in $\mathcal{D}_2$ that are far from $x_{\mathcal{L}}$.

At this point in the algorithm, we also update the set $\mathcal{X}$ by adding to it the states in $\mathcal{X}_{\text{new}}$. We do the same for the corresponding set of controls $\mathcal{V}$. We then feed the updated $\mathcal{X}$ and $\mathcal{V}$ back into the RRNN and the algorithm begins a new iteration.

4. CONTROLLER SYNTHESIS PHASE

After the dynamic training procedure completes, we obtain the set of states $\mathcal{X}$ near $\bar{x}$ and corresponding controls $\mathcal{V}$. From each state $\hat{x}_i \in \mathcal{X}$ and control function $\hat{u}_i(\cdot) \in \mathcal{V}$, we directly have the approximate TTR values: $\hat{\phi}(x_i) = \hat{T}_i$. These approximate TTR values can be used to synthesize a control at $\bar{x}$ according to (6). However, in order to bring the system from $\bar{x}$ all the way to $x_{\mathcal{L}}$, a few more post-processing steps are needed.

4.1 Trajectory Tracing

In order to drive the system from $\bar{x}$ to $x_{\mathcal{L}}$, gradient information is necessary at points between $\bar{x}$ and $x_{\mathcal{L}}$ along a dynamically feasible trajectory. Fortunately, this information can be computed from $\mathcal{X}$ and $\mathcal{V}$. Specifically, each $\hat{x}_i \in \mathcal{X}$ and $\hat{u}_i(\cdot) \in \mathcal{V}$ produce a trajectory $\xi_i^f(t; \hat{x}_i, 0, \hat{u}_i(\cdot)), t \in [0, \hat{T}_i]$. From the trajectories, we can obtain M_T states on the trajectory by discretizing the time t into M_T time points. We denote these states $x_{(i,j)}$, where the index i comes from the index of $\hat{x}_i \in \mathcal{X}$, and the index $j \in \{0, \ldots, M_T - 1\}$ indicates that the state is computed from the jth time point on the trajectory ξ_i^f. Mathematically, $\hat{x}_{(i,j)}$ is given as follows:

$$\begin{aligned} \hat{x}_{(i,j)} &= \xi_i(t_j; \hat{x}_i, 0, \hat{u}_i(\cdot)), \\ t_j &= \frac{j\hat{T}_i}{M_T - 1}, j = 0, 1, \ldots, M_T - 1 \end{aligned} \tag{11}$$

The trajectory tracing process is summarized in Alg. 3, where we have denoted the set $\{x_{(i,j)}\}$ as $\bar{\mathcal{X}}$.

4.2 Imposing a Grid

While the source of the exponential time and space complexity problem lies in discretization of the state space, imposing a grid can still be useful as long as the number of grid points is small. Thus, we organize the approximate TTR values $\hat{\phi}(x), x \in \bar{\mathcal{X}}$ by imposing a small grid $\mathcal{G}(x)$ around a state x at which the a control needs to be synthesized, starting with $x = \bar{x}$. As the system moves from $\bar{x}$ to $x_{\mathcal{L}}$, we move the grid $\mathcal{G}(x)$ along so that it is always centered at the current system state $x(t)$ and has a resolution suitable for the local density of points near x in $\bar{\mathcal{X}}$. This is computationally feasible since the grid does not cover a large part of the state space.

After the local grid $\mathcal{G}(x)$ is created, each state $\hat{x}_i$ that lies within the bounds of $\mathcal{G}(x)$ gets mapped to the nearest grid point. Depending on the resolution of $\mathcal{G}(x)$ and the

Algorithm 2 Dynamic Training

Results: states near $\bar{x}$, $\mathcal{X}$; corresponding controls, $\mathcal{V}$
Inputs: $\bar{x}$, ϵ, M_ϵ, $\text{iter}_{\max}$, $M_{\max}$, iter_{ps}, $\mathcal{D}_2$, $\mathcal{R}_{\text{O}}$, $\mathcal{R}_{\text{PS}}$, $\mathcal{R}_{\text{ITS}}$
Initialization:
$\mathcal{X} = \mathcal{D}_2$, iter $= 0$
$\mathcal{E} \leftarrow M_\epsilon$ uniformly sampled states from ϵ-ball around $\bar{x}$
while iter $<$ $\text{iter}_{\max}$ **do**
  iter $\leftarrow$ iter $+ 1$
  $\mathbb{W} \leftarrow \text{trainNN}(\mathcal{X}, \mathcal{V})$
  NN output filtering:
  $\mathcal{V}_{\text{new}}, \mathcal{X}_{\text{new}} \leftarrow \emptyset$
  for $x_i \in \mathcal{E}$ **do**
    $\hat{u}(\cdot) \leftarrow \hat{g}(x_i, x_{\mathcal{L}}; -f(\cdot,\cdot), \mathbb{W})$
    $\mathcal{V}_{\text{new}} \leftarrow \mathcal{V}_{\text{new}} \cup \{(\hat{u}(\cdot)\}$
  end for
  for $\hat{u}_i(\cdot) \in \mathcal{V}_{\text{new}}$ **do**
    $\mathcal{X}_{\text{new}} \leftarrow \mathcal{X}_{\text{new}} \cup \{\xi(\hat{T}; x_{\mathcal{L}}, 0; \hat{u}_i(\cdot))\}$
  end for
  for $x_i \in \mathcal{X}_{\text{new}}$ **do**
    $A =$ Filter$(x_i, \mathcal{R}_{\text{O}})$
    if $!A$ **then**
      $\mathcal{X}_{\text{new}} \leftarrow \mathcal{X}_{\text{new}} \setminus x_i$
      $\mathcal{V}_{\text{new}} \leftarrow \mathcal{V}_{\text{new}} \setminus u_i$ (corresponding control)
    end if
  end for
  Previous state filtering:
  for $x_i \in \mathcal{X}$ **do**
    $A =$ Filter$(x_i, \mathcal{R}_{\text{PS}})$
    if $!A$ **then**
      $\mathcal{X} \leftarrow \mathcal{X} \setminus x_i$
      $\mathcal{V} \leftarrow \mathcal{V} \setminus u_i$ (corresponding control)
    end if
  end for
  Initial training set filtering:
  if iter $>$ iter_{ps} **then**
    for $x_i \in \mathcal{X} \cap \mathcal{D}_2$ **do**
      $A =$ Filter$(x_i, \mathcal{R}_{\text{ITS}})$
      if $!A$ **then**
        $\mathcal{X} \leftarrow \mathcal{X} \setminus x_i$
        $\mathcal{V} \leftarrow \mathcal{V} \setminus u_i$ (corresponding control)
      end if
    end for
  end if
  $\mathcal{X} \leftarrow \mathcal{X} \cup \mathcal{X}_{\text{new}}$
  $\mathcal{V} \leftarrow \mathcal{V} \cup \mathcal{V}_{\text{new}}$
  if $|\{x \in \mathcal{X} : \|x - x_{\mathcal{L}}\|_2 \leq \epsilon\}| \geq M_{\max}$ **then**
    return
  end if
end while

Algorithm 3 Trajectory Tracing

Result: Points in region around dynamically feasible trajectory, $\bar{\mathcal{X}}$
Inputs: $\mathcal{X}$, $\mathcal{V}$, M_T
Initialization: $\bar{\mathcal{X}} \leftarrow \emptyset$
Algorithm:
for $\hat{x}_i \in \mathcal{X}$ **do**
  for $j \in \{0, 1, \ldots, M_T - 1\}$ **do**
    compute $\hat{x}_{(i,j)}$ using (11)
    $\bar{\mathcal{X}} \leftarrow \bar{\mathcal{X}} \cup \{\hat{x}_{(i,j)}\}$
  end for
end for

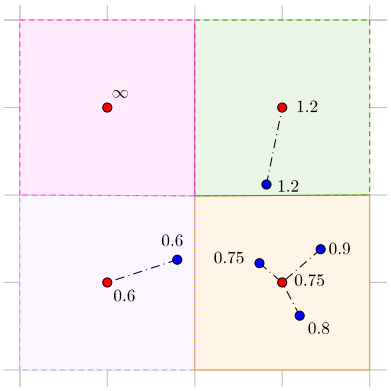

Figure 3: Red: grid points $\hat{x}_{(i,j)}$; blue: states $\hat{x}_i$ from $\bar{\mathcal{X}}$; numbers: minimized TTR value $\hat{\phi}(x_{(i,j)})$ at grid point $\phi(x_{(i,j)})$(red), TTR value $\hat{\phi}(x_i)$ of state $\hat{x}_i$ (blue)

density of $\bar{\mathcal{X}}$ around x, multiple states $\{x_{(i,j)}\} \subset \bar{\mathcal{X}}$ may be mapped to the same grid point, which for convenience we will denote $x_{\mathcal{G}}$. When this occurs, we assign $\hat{\phi}(x_{\mathcal{G}})$ to be the minimum out of the corresponding TTR approximations $\hat{\phi}(\hat{x}_{(i,j)})$. If no points are mapped to some grid point $x_{\mathcal{G}}$, then $\hat{\phi}(x_{\mathcal{G}}) = \infty$ for that point.

Fig. 3 illustrates the process of imposing the grid. Blue dots correspond to states $\hat{x}_{(i,j)} \in \bar{\mathcal{X}}$, and numbers adjacent to the blue dots represent $\hat{\phi}(\hat{x}_{(i,j)})$. Red dots correspond to grid points, and the adjacent number represents $\hat{\phi}(\hat{x}_{(i,j)})$. The shaded region surrounding each grid point corresponds to the locations in which states are mapped to that particular grid point.

4.3 Smart Gradient Approximation

The next step for driving the system to $x_{\mathcal{L}}$ is computing the gradients of the approximate TTR function, $\nabla\hat{\phi}(x)$, so that (6) can be used. Since we have the grid $\mathcal{G}(x)$ and approximate TTR values $\hat{\phi}(x)$ on the grid, standard numerical methods for computing the gradient can in principle be used. However, depending on the set $\bar{\mathcal{X}}$, in general not every grid point of $\mathcal{G}(x)$ can be assigned a $\hat{\phi}(x)$.

Alg. 4 provides a heuristic for approximating the gradient on a grid whose grid points do not all contain a function value. This is done by selecting grid points near x carefully based on the availability of function value, and then approximating a component of the gradient by taking a first-order forward, backward, or central difference. When needed, function values are extrapolated.

In the algorithm, we assume that the gradient in kth component, $\nabla_k\hat{\phi}(x)$ is computed. The functions in the algorithm are named according to their output and are simple to implement. These are listed below:

- data_above, data_below: returns all available points on $\mathcal{G}$ respectively "above" and "below" x in the kth component.
- closest_above, closest_below: returns the closest point on $\mathcal{G}$ respectively "above" and "below" x in the kth component.
- second_closest_above, second_closest_below: returns the second closest point on $\mathcal{G}$ respectively "above" and "below" x in the kth component.

4.4 Control Computation

Repeatedly using Alg. 4 for all the components of the system dimension, we can obtain $\nabla\hat{\phi}(x)$, from which a suboptimal control can be computed via (6). In practice, depending on how the control appears in the system dynamics, some components of the gradients may not be needed to derive a control. In this case, only the gradient components necessary for computing the control according to (6) are needed.

Algorithm 4 Gradient Approximation

Result: $\nabla_k\hat{\phi}(x)$
Inputs: $\mathcal{G}, \{\hat{\phi}(\hat{x}_{(i,j)})\}, \bar{\mathcal{X}}$
Initialization:
above $\leftarrow$ data_above$(\mathcal{G}, \bar{\mathcal{X}})$
below $\leftarrow$ data_below$(\mathcal{G}, \bar{\mathcal{X}})$
if |above|! $= 0$ **and** |below|! $= 0$ **then**
  $x_+ \leftarrow$ closest_above$(\mathcal{G}, \bar{\mathcal{X}})$
  $x_- \leftarrow$ closest_below$(\mathcal{G}, \bar{\mathcal{X}})$
else if |above| == 0 **and** |below|! $= 0$ **then**
  if |below| < 2 **then**
    $\nabla_k\hat{\phi}(x) \leftarrow \infty$
    return
  else
    $x_+ \leftarrow$ closest_below$(\mathcal{G}, \bar{\mathcal{X}})$
    $x_- \leftarrow$ second_closest_below$(\mathcal{G}, \bar{\mathcal{X}})$
  end if
else if |below| == 0 **and** |above|! $= 0$ **then**
  if |above| < 2 **then**
    $\nabla_k\hat{\phi}(x) \leftarrow -\infty$
    return
  else
    $x_+ \leftarrow$ second_closest_above$(\mathcal{G}, \bar{\mathcal{X}})$
    $x_- \leftarrow$ closest_above$(\mathcal{G}, \bar{\mathcal{X}})$
  end if
else
  $\nabla_k\hat{\phi}(x)$ cannot be determined
end if
$\nabla_k\hat{\phi}(x) \leftarrow \frac{\hat{\phi}(x_+) - \hat{\phi}(x_-)}{x_+ - x_-}$

5. DUBINS CAR EXAMPLE

5.1 Vehicle Dynamics

Consider the Dubins Car, with state $x = (p_x, p_y, \theta)$. (p_x, p_y) are the x and y positions of the vehicle, and θ is the heading

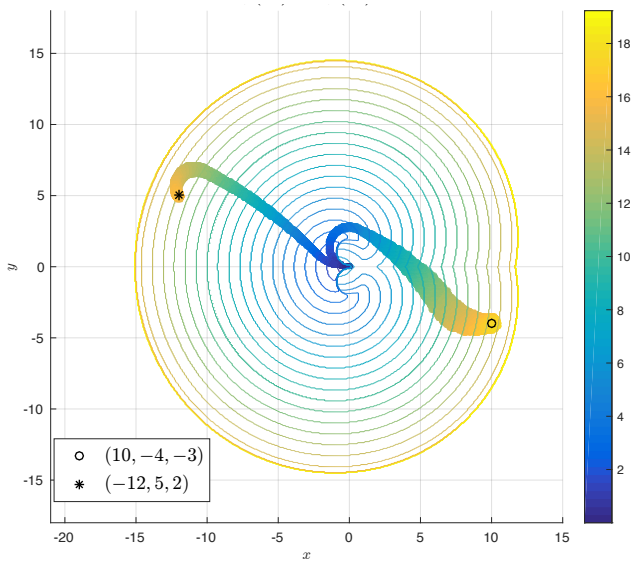

Figure 4: Comparison of the true TTR function $\phi(x)$ computed over a large portion of the state space, and the approximate TTR from our NN-based approach $\hat{\phi}(x)$ on two different corridors containing the initial state $\bar{x}$, the target set $x_{\mathcal{L}}$, and a dynamically feasible trajectory. The contours are level sets of $\phi(x)$. Two different corridors in which $\hat{\phi}(x)$ is computed resulting from two different values of $\bar{x}$ $((10, -4, -3), (-12, 5, 2))$ are also plotted using the same colormap.

of the vehicle. The system dynamics, assuming unit longitudinal speed, are

$$\begin{aligned} \dot{p}_x &= \cos\theta \\ \dot{p}_y &= \sin\theta \\ \dot{\theta} &= u, \qquad |u| \leq 1 \end{aligned} \tag{12}$$

The control of the Dubins car is denoted u, and is constrained to lie in the interval $[-1, 1]$, the interpretation of which is that the vehicle has a maximum turn rate of 1 rad/s. We choose the Dubins car to illustrate our method because of the simple structure of the optimal controls. In addition, since the model is only 3D, we are able to verify our results by comparing them to the those obtained via HJ reachability.

For our example, we have chosen many different initial states $\bar{x}$ for the system. The target state $x_{\mathcal{L}}$ is chosen as the origin.

5.2 Control Primitives

In [19], the author shows that all optimal trajectories of the Dubins car utilize controls that represent going straight or turning maximally left or right. Thus, the set of controls that are valid for generating optimal trajectories can be reduced down to three motion primitives, {'L', 'S', 'R'}, encoding the controls $u = 1$ (max left), $u = 0$ (straight), and $u = -1$ (max right) respectively. Furthermore, [19] also shows that for any given $\bar{x}$ and $x_{\mathcal{L}}$, the optimal control is a sequence of at most three of these motion primitives. In other words, the optimal control for any given target state is simply a permutation of {'L', 'S', 'R'} with an appropriate time duration associated with each primitive. Since these motion primitives correspond to arcs and line segments, the optimal trajectories for Dubins car can be geometrically interpreted as concatenated sequences of arcs and line segments.

Following our notation in Section 3, any optimal control sequence can be written as $\{u^1, u^2, u^3\}, \{\tau^1, \tau^2, \tau^3\}$ where u^i denotes the ith control primitive and τ^i denotes the duration of ith control primitive. We choose u^i from the three possible optimal values $\{-1, 0, 1\}$. The initial dataset $\mathcal{D}_2$ for dynamic training is composed of control primitives with duration randomly sampled from the interval $[0, T], T = 2\pi$. With our choice of T, the maximum time horizon considered is then $3T = 6\pi$.

5.3 Neural Network

Using the RRNN architecture described in Section 3.1, we let $N = 3$, since we only need at most three control primitives. Since the controls and dynamics of Dubins car are simple, we have chosen the hidden sizes of P, D, U, X to be $[10, 10, 6, 75]$, respectively. The NN is trained with the training functionality of the MATLAB Neural Network ToolBox 2016. The training function used for the full NN is resilient back-propagation and the performance function used is mean squared error.

5.4 Neural Network Training

Running the dynamic training algorithm on even the low-dimensional Dubins Car results in significant memory usage savings compared to using dynamic programming-based methods. As the NN learns the inverse backward system dynamics g, a dynamically feasible "corridor" between the initial state $\bar{x}$ and target state $x_{\mathcal{L}}$ is picked out, as shown in Fig. 4. Without our proposed method, if one chooses some arbitrary region enclosing $\bar{x}$ and $x_{\mathcal{L}}$, and naively computes the TTR function $\phi(x)$ using level set methods, it is unlikely that the a solution can be found throughout the entire corridor, since the region may not contain dynamically feasible trajectories.

Before dynamic training, we first initialize the weights W_X. This is done using the dataset $\mathcal{D}_1$, which is generated by random sampling. Exploiting the fact that there are only six optimal control primitives for the Dubins car, we sample the $u = \pm 1$ primitives 25 times less frequently than the $u = 0$ primitive. For the possible durations of each primitive, τ^i, we randomly sampled in the interval $[0, T], T = 100$ according to a linearly increasing probability distribution on $[0, T]$. This distribution is chosen so that starting from $x_{\mathcal{L}}$, the backward dynamics drive the system to a relatively uniform distribution of states $\bar{x}$.

For generating the dataset $\mathcal{D}_2$, we follow a similar procedure to generating $\mathcal{D}_1$, except we sample time durations τ^i in the interval $[0, T], T = 2\pi$.

To initialize the dynamic training process, we chose $\epsilon = 1$, and $M_\epsilon = 500$, $\text{iter}_{\max} = 50$, $M_{\max} = 10000$, $\text{iter}_{\text{ps}} = 5$.

5.4.1 *Filtering Algorithms*

For the exponential filtering process, $\mathcal{R}_O$ is chosen to be the cone of minimum size that contains the epsilon ball, with the tip of the cone located at $\bar{x}$. The choice of using a conical filter is based on the hypothesis that a trajectory taking the system from $\bar{x}$ to $x_{\mathcal{L}}$ is likely to stay in the cone $\mathcal{R}_O$. $\mathcal{R}_{\text{PS}}$ was chosen to be a sphere around $\bar{x}$ to serve as a

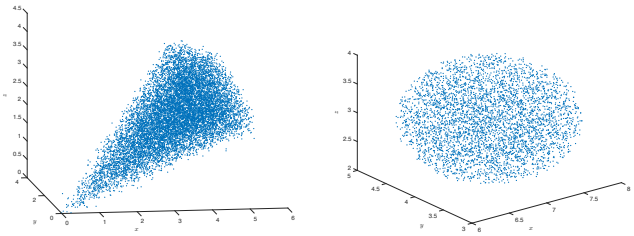

(a) (b)

Figure 5: Accept regions for filtering during the dynamic training process. (a) shows the cone filter when $\bar{x} = (4.2, 2.3, 2.6)$. (b) shows the spherical target filter when $\bar{x} = (7, 4, 3)$.

more stringent filter than the cone filter. $\mathcal{R}_{\text{ITS}}$ was chosen to be a spherical target filter as well, since the initial training set is supposed to be pruned only when the NN has already learned to drive the system to $\bar{x}$ reasonably well. The conical and spherical target filters are shown in Fig. 5a and Fig. 5b respectively.

5.4.2 *Filter Decay Rate: Setting and Timing*

Although $\mathcal{R}_{\text{O}}, \mathcal{R}_{\text{PS}}, \mathcal{R}_{\text{ITS}}$ are chosen before the dynamic training process, the filtering of the training set $\mathcal{X}$ can still be adjusted while training. This is done by varying the parameters $\lambda_{\text{O}}, \lambda_{\text{PS}}, \lambda_{\text{ITS}}$. In early training iterations, we want to decrease λ_{O} slightly to ensure that we are not filtering out states needed for the NN to explore the state space. Once the NN has gained a better understanding of how to reach $\bar{x}$, we increase λ_{O} and λ_{ITS} slightly to further encourage the NN to drive states near $\bar{x}$. When the dataset is mostly near $\bar{x}$, we increase λ_{PS} and λ_{ITS} significantly.

5.5 Dubins Car Results

5.5.1 *Training Process*

In Fig. 6a, 6b, 6c, the process by which the training set $\mathcal{X}$ changes from the initial training set $\mathcal{D}_2$ to an ϵ-ball around $\bar{x} = (15, 12, 3)$ is shown. Here, the red states represent the set $\mathcal{E}$ and the black states represent the states in $\mathcal{X}$. In the

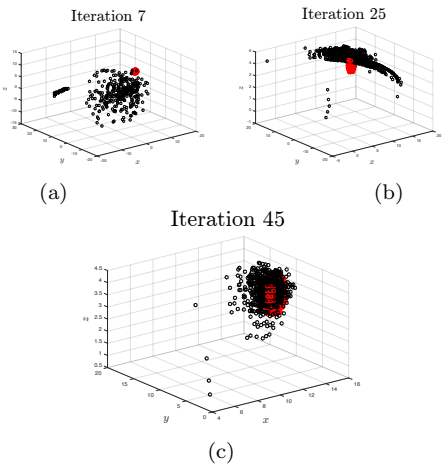

(a) (b) (c)

Figure 6: Evolution of $\mathcal{X}$ over many iterations.

State $\bar{x}$	NN TTR $\hat{\phi}(\bar{x})$	True TTR $\phi(\bar{x})$
$(-12, 5, 2)$	15.20	14.84
$(-10, 0, 0)$	10.01	10.00
$(1, 1, 6)$	7.45	7.40
$(10, -4, -3)$	16.51	13.36
$(30, 15, 3)$	56.79	?

Table 1: Trajectory times (seconds)

early iterations (Fig. 6a), the NN explores outward from the initial training set, frequently making mistakes, resulting in the states in $\mathcal{X}$ being very far away from $\bar{x}$. As the iteration number increases, the training set $\mathcal{D}_2$ is filtered out, and eventually the NN tends to output controls $\hat{u}_i(\cdot)$ that produces states $\hat{x}_i$ in an arc. This can be seen in Fig. 6b. By the end of the training process, the $\mathcal{R}_O$ conical target filter prunes the states outside of the ϵ-ball. This can be seen in Fig. 6c.

5.5.2 *TTR Value Comparison*

The true TTR values $\phi(x)$ and the approximate TTR values $\hat{\phi}(x)$ determined by the NN output of several states are compared in Table 1.

The difference between $\phi(x)$ and $\hat{\phi}(x)$ is not very large. In fact, $\hat{\phi}(x)$ is sometimes even smaller than $\phi(x)$. Our method guarantees that $\hat{\phi}(x)$ is a conservative approximation – an over-approximation. The larger $\phi(x)$ values are likely due to numerical error in the level set methods used. In our particular example, the target set is a single state, making a level set representation of the target set very difficult. However, a singleton target set does not limit our NN-based approach in any way.

5.5.3 *Computation Complexity*

Synthesizing control using our NN-based approach allows for large time complexity improvements in comparison to using level set methods. On a 2012 MacBook Pro laptop, data generation requires approximately 3 minutes, and controller synthesis from this data and simulation requires approximately 23 minutes. Since the region of the state space we are considering is quite large, and the target set is quite small (a singleton), the level set methods approach is intractable on this laptop, and requires 4 days on a desktop computer with a Core i7-5820K processor and 128 GB of RAM.

There are also large spatial savings by using the NN. For example, $\mathcal{X}$ and $\hat{\phi}(x), x \in \mathcal{X}$ for one particular corridor computed between $(10, -1, -3)$ and $(0, 0, 0)$ requires only 179 MB of RAM, while a reachable set computed over that horizon on a very low resolution grid requires approximately 7 GB of RAM.

As can be seen from this and the previous sections, using level set methods not only is more time-consuming compared to using our NN-based approach, but also does not guarantee a more shorter trajectory due to discretization error.

6. CONCLUSIONS AND FUTURE WORK

Our NN-based grid-free method computes an upper bound of the optimal TTR function in a region of the state space that contains the initial state, the target set, and a feasible trajectory. By combining the strengths of dynamic programming-based and machine learning-based approaches,

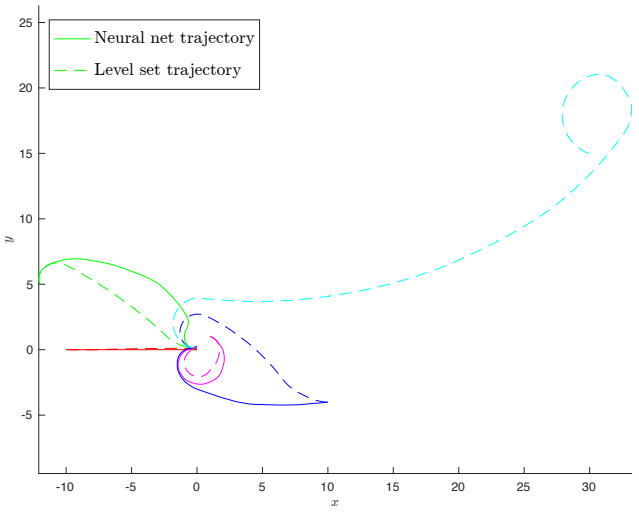

Figure 7: Trajectories generated using level set methods (dashed) and using our NN-based method (solid). Each color corresponds to a different initial state $\bar{x}$.

we greatly alleviate the curse of dimensionality while maintaining a desired direction of conservatism, effectively avoiding the shortcomings of both types of approaches.

Using a numerical example, we demonstrate that our approach can successfully generate near-optimal TTR values in multiple test cases for the Dubins car. Due to our method being grid-free, in some cases the estimated TTR values are even smaller than the those computed by level set methods, which suffer from discretization error. In addition, we are able to approximate TTR values in regions that are very far from the target set, a very computationally expensive task for dynamic programming-based approaches. Our approximate TTR function is able to drive the Dubins car from many different initial conditions to the target set.

Although our current results are promising, much more investigation is still needed to make our approach more practical and applicable to more scenarios. For example, better intuition for the choice of accept regions in the filtering process is needed to extend our approach to other systems. We currently plan to investigate applying our method to the 6D engine-out plane [1] as well as a 12D quadrotor model. In addition to path planning, we also hope to extend our theory to provide safety guarantees and robustness against disturbances. Such extensions are non-trivial due to the different roles that the control and disturbance inputs play in the system dynamics.

7. REFERENCES

[1] Adler, A., Bar-Gill, A., and Shimkin, N. Optimal flight paths for engine-out emergency landing. In *Proceedings of the 2012 24th Chinese Control and Decision Conference, CCDC 2012* (may 2012), IEEE, pp. 2908–2915.

[2] Allen, R. E., Clark, A. A., Starek, J. A., and Pavone, M. A Machine Learning Approach for Real-Time Reachability Analysis Ross. In *International Conference on Intelligent Robots and Systems* (sep 2014), no. Iros, IEEE, pp. 2202–2208.

[3] Amazon. Amazon Prime Air. http://www.amazon.com/b?node=8037720011. Accessed: 2016-10-09.

[4] AUVSI News. UAS Aid in South Carolina Tornado Investigation. http://www.auvsi.org/blogs/auvsi-news/2016/01/29/tornado. Accessed: 2016-10-09.

[5] Barron, E. N. Differential games with maximum cost. *Nonlinear Analysis 14*, 11 (jun 1990), 971–989.

[6] Barron, E. N., and Ishii, H. The Bellman equation for minimizing the maximum cost. *Nonlinear Analysis 13*, 9 (1989), 1067–1090.

[7] BBC News. Google plans drone delivery service for 2017. http://www.bbc.co.uk/news/technology-34704868, 2015. Accessed: 2016-10-09.

[8] Becerikli, Y., Konar, A. F., and Samad, T. Intelligent optimal control with dynamic neural networks. *Neural networks : the official journal of the International Neural Network Society 16*, 2 (mar 2003), 251–9.

[9] Bokanowski, O., Forcadel, N., and Zidani, H. Reachability and Minimal Times for State Constrained Nonlinear Problems without Any Controllability Assumption. *SIAM Journal on Control and Optimization 48*, 7 (jan 2010), 4292–4316.

[10] Bokanowski, O., and Zidani, H. Minimal time problems with moving targets and obstacles. *IFAC Proceedings Volumes (IFAC-PapersOnline) 18*, PART 1 (2011), 2589–2593.

[11] Chen*, M., Herbert*, S., and Tomlin, C. J. Fast Reachable Set Approximations via State Decoupling Disturbances. In *55th IEEE Conference on Decision and Control (to appear)* (2016).

[12] Chen, M., Hu, Q., Mackin, C., Fisac, J. F., and Tomlin, C. J. Safe platooning of unmanned aerial vehicles via reachability. In *2015 54th IEEE Conference on Decision and Control (CDC)* (dec 2015), vol. 2016-Febru, IEEE, pp. 4695–4701.

[13] Crandall, M. G., and Lions, P.-l. Viscosity solutions of Hamilton-Jacobi equations. *Transactions of the American Mathematical Society 277*, 1 (jan 1983), 1–1.

[14] Cybenko, G. Approximation by Superposition of a Sigmoidal Function.

[15] Darbon, J., and Osher, S. Algorithms for overcoming the curse of dimensionality for certain HamiltonâĂŞJacobi equations arising in control theory and elsewhere. *Research in the Mathematical Sciences 3*, 1 (dec 2016), 19.

[16] Ding, J., Sprinkle, J., Sastry, S. S., and Tomlin, C. J. Reachability calculations for automated aerial refueling. In *Proceedings of the IEEE Conference on Decision and Control* (Cancun, Mexico, 2008), pp. 3706–3712.

[17] Djeridane, B., and Lygeros, J. Neural approximation of PDE solutions: An application to reachability computations. In *Proceedings of the 45th IEEE Conference on Decision and Control* (2006), IEEE, pp. 3034–3039.

[18] Dreossi, T., Dang, T., and Piazza, C. Parallelotope Bundles for Polynomial Reachability. In

Proceedings of the 19th International Conference on Hybrid Systems: Computation and Control - HSCC '16 (New York, New York, USA, 2016), ACM Press, pp. 297–306.

[19] Dubins, L. E. On Curves of Minimal Length with a Constraint on Average Curvature, and with Prescribed Initial and Terminal Positions and Tangents. *American Journal of Mathematics 79*, 3 (jul 1957), 497–516.

[20] Evans, L. C., and Souganidis, P. E. Differential games and representation formulas for solutions of {Hamilton-Jacobi-Isaacs} equations. *Indiana Univ. Math. J. 33*, 5 (1984), 773–797.

[21] Fehrenbacher, K. Feds Say Safety Is the Key to the Future of Autonomous Cars. http://fortune.com/2016/07/19/safety-feds-autonomous-cars/. Accessed: 2016-10-09.

[22] Fisac, J. F., Chen, M., Tomlin, C. J., and Sastry, S. S. Reach-avoid problems with time-varying dynamics, targets and constraints. In *Proceedings of the 18th International Conference on Hybrid Systems Computation and Control - HSCC '15* (New York, New York, USA, 2015), ACM Press, pp. 11–20.

[23] Joint Planning and Development Office. Unmanned Aircraft Systems (UAS) Comprehensive Plan: A Report on the Nation's UAS Path Forward. Tech. rep., 2013.

[24] Kim, B. S., and Calise, A. J. Nonlinear Flight Control Using Neural Networks. *Journal of Guidance, Control, and Dynamics 20*, 1 (jan 1997), 26–33.

[25] Kopardekar, P., Rios, J., Prevot, T., Johnson, M., Jung, J., and Iii, J. E. R. Unmanned Aircraft System Traffic Management (UTM) Concept of Operations. *16th AIAA Aviation Technology, Integration, and Operations Conference*, 1–16.

[26] Majumdar, A., Vasudevan, R., Tobenkin, M. M., and Tedrake, R. Convex optimization of nonlinear feedback controllers via occupation measures. *The International Journal of Robotics Research 33*, 9 (aug 2014), 1209–1230.

[27] Margellos, K., and Lygeros, J. Hamilton-Jacobi Formulation for Reach-Avoid Differential Games. *IEEE Transactions on Automatic Control 56*, 8 (aug 2011), 1849–1861.

[28] McGrew, J., Bush, L., How, J., Roy, N., and Williams, B. Air Combat Strategy Using Approximate Dynamic Programming. *AIAA Guidance, Navigation and Control Conference and Exhibit* (aug 2008), 1–33.

[29] Mitchell, I. A toolbox of level set methods. Tech. rep., 2007.

[30] Mitchell, I. M., Bayen, A. M., and Tomlin, C. J. A time-dependent Hamilton-Jacobi formulation of reachable sets for continuous dynamic games. *IEEE Transactions on Automatic Control 50*, 7 (2005), 947–957.

[31] Mitchell, I. M., and Tomlin, C. J. Overapproximating Reachable Sets by Hamilton-Jacobi Projections. *Journal of Scientific Computing 19*, 1-3 (2003), 323–346.

[32] Niarchos, K. N., and Lygeros, J. A Neural Approximation to Continuous Time Reachability Computations. In *Proceedings of the 45th IEEE Conference on Decision and Control* (2006), IEEE, pp. 6313–6318.

[33] Osher, S., and Fedkiw, R. *Level Set Methods and Dynamic Implicit Surfaces*. Springer-Verlag, 2006.

[34] Sethian, J. A. A fast marching level set method for monotonically advancing fronts. *Pnas 93*, 4 (1996), 1591–1595.

[35] Tomlin, C. J., Lygeros, J., and Sastry, S. A Game Theoretic Approach to Controller Design for Hybrid Systems. *Proceedings of IEEE 88*, 7 (jul 2000), 949–969.

[36] Varaiya, P. On the existence of solutions to a differential game. *SIAM Journal on Control 5*, 1 (1967), 153–162.

[37] Yang, I., Becker-Weimann, S., Bissell, M. J., and Tomlin, C. J. One-shot computation of reachable sets for differential games. In *Proceedings of the 16th international conference on Hybrid systems: computation and control - HSCC '13* (New York, New York, USA, 2013), ACM Press, p. 183.